Hindawi
Advances in Civil Engineering
Volume 2021, Article ID 5555436, 13 pages
https://doi.org/10.1155/2021/5555436

Research Article

Investigation of Freeze-Thaw Resistance of Stabilized Saline Soil

Yongxiang Zhou[1,2,3] **Qingfeng Guan**[1,2,3] **and Peiyu Yan**[4]

[1]*Institute of Building Materials, China Academy of Building Research, Beijing 100013, China*
[2]*State Key Laboratory of Building Safety and Built Environment, Beijing 100013, China*
[3]*National Engineering Research Center of Building Technology, Beijing 100013, China*
[4]*Department of Civil Engineering, Tsinghua University, Beijing 100084, China*

Correspondence should be addressed to Yongxiang Zhou; zhouyxt@126.com

Received 27 January 2021; Revised 6 March 2021; Accepted 25 March 2021; Published 7 April 2021

Academic Editor: Tingting Zhang

Copyright © 2021 Yongxiang Zhou et al. This is an open access article distributed under the Creative Commons Attribution License, which permits unrestricted use, distribution, and reproduction in any medium, provided the original work is properly cited.

In this paper, three freezing-thawing tests are designed to study the freeze-thaw resistance of stabilized sulfate type saline soil. The results show that different destructive modes and erosion extents are caused by different freeze-thaw conditions. The destructive effect from salt tends to be limited if there is no external water intrusion. When sufficient water is provided, ice expansion, dissolution recrystallization of salts, and ettringite growth during the thawing phase may take place. Soil water potential is used for analysis and explanation of the driving force and water migration in the stabilized soil. Pressure potential caused by the air sealed in the stabilized soil specimen leads to early water concentration in the outer parts of the specimen, and the surface layer is first eroded under the freeze-thaw cycles. A high percentage of soil stabilizer can improve the freeze-thaw resistance of stabilized soil, but a sufficiently long curing period plays a more important role. This study provides useful insights for improving the freeze-thaw resistance of solidified saline soil in road engineering.

1. Introduction

There is a large amount of inland saline soil distributed widely in northwest China. Saline soil is a type of soil whose salt content exceeds a certain threshold, and some common classifications include chlorine saline soil, sulfate saline soil, and carbonate saline soil. Among these, sulfate saline soil occupies the largest area in northwest China and is most harmful for roadbed engineering [1]. It may be necessary to build roads in saline soil zones due to exploration and exploitation of mineral resources such as salt lakes. However, the content of soluble chloride and sulfate salt in saline soil is very high, and the mass percent of saline soil may exceed 30%, which can often cause road engineering hazards such as dissolution, salt expansion, frost damage, and frost heaving [2–4]. In a harsh saline soil environment, ordinary concrete will severely corrode, and its service life is only a few years. Such a harsh environment will pose a severe threat to the durability of ordinary concrete and severely limit the feasibility of using concrete for construction.

One of the most effective technical solutions is to use stabilized saline soil as a base or subbase of roads, sometimes even as a pavement for low-grade roads. Methods of soil stabilization can generally be divided into physical reinforcement (mechanical force stabilization and heat treatment stabilization) [5, 6], chemical stabilization (trinity mixture fill stabilization, modern curing agent stabilization, salt solution, and asphalt stabilization) [7–10], and biological stabilization (microbiologically induced calcite precipitation, MICP) [11–15]. The relevant properties of stabilized soil have undergone significant improvement, and application technologies of stabilized soil are becoming increasingly advanced [16, 17].

It should be noted that the environment in northwest China is harsh, with hot summers and dry and cold winters, especially in the northwest of Qinghai-Tibet plateau where the sunshine is strong, the annual average temperature is below 5.1°C, and the temperature difference between day and night is high with an extreme minimum temperature of −29°C to −34°C [18]. During the long winters, highway

engineering structures experience severe freeze-thaw cycles many times. Similar to expansive clay, saline soil has a high sodium sulfate content that may expand or shrink through crystallization or dissolution with moisture change. It also has the properties of relatively high solubility and corrosivity. In cold areas, road and railroad engineers need to consider problems such as roadbed swelling and frost boiling resulting from the presence of sulfate saline soil [19].

Many previous studies have investigated the damage mechanism of the freeze-thaw cycle in saline soil in cold areas. In a cold environment, the migration and accumulation of free water in saline soil are affected by the cooling rate and temperature gradient [20]. The freezing of water in saline soil is a dynamic process of hydrothermal and salt-mechanical interaction [21, 22]. It has been reported that the frost deformation of saline soil can be divided into three steps [23]. The first is a salt heaving period when the temperature is higher than the freezing point of water; sodium sulfate will form, and the amount of free water decreases as the temperature decreases. The second step is a salt heaving and frost heaving period when the temperature is between the freezing point and the salt swelling temperature. Hence, salt heave and frost heave occur at the same time, resulting in a rapid volume expansion. The last step is the frost heaving period when the temperature continues to decrease and is lower than the salt swelling temperature, and finally the frost heaving appears. To investigate the mechanism of the salt heaving effect on saline soil, previous studies [24, 25] have proposed a thermo-hydro-salt-mechanical coupled model considering a phase change and stated that the most important method for the protection of constructions in saline soil areas is to effectively prevent the migration, accumulation, and phase change of water and salt [26, 27].

Based on existing research [17, 28, 29] on saline soil such as salt crystallization, salt and water transfer, salt deformation and frost heave, and a water-heat-salt coupled model, many researchers [7, 16, 30, 31] have conducted investigations to improve the freezing resistance of saline soil. However, these have been for natural saline soil. The freezing resistance of stabilized saline soil, especially saline soil stabilized by cement-based materials, has not yet received sufficient attention, and the understanding of mechanisms such as freeze-thaw damage and improvement of freezing resistance deserves further attention. There is no special test or standard to evaluate the freezing resistance of stabilized saline soil, which is not conducive to promoting the use of saline soil stabilized by cement-based material in severe cold areas. Successfully stabilizing saline soil and improving its durability are of important significance for solving road traffic problems in the saline soil areas in northwest China.

Herein, we therefore study the freezing resistance of saline soil stabilized by cement-based materials. We focus on salt crystallization, salt and water transfer, and the migration driving force of stabilized saline soil under different methods of water supply in freezing and thawing conditions. We firstly design three types of water supply tests and transfer the cured samples of stabilized saline soil of different ages into a freezer to undergo different freeze-thaw cycles. Then, we record the appearance and measure the unconfined compressive strength and cumulative mass loss of samples. Finally, we introduce a soil water potential model to explain the damage mechanism and failure mode of stabilized saline soil under different water supply methods.

2. Materials and Test Methods

2.1. Saline Soil. A typical natural sulfate saline soil from Golmud, Qinghai Province, China, was used in this study. This soil is local salinized clay that contains about 4% soluble salts (mainly sodium sulfate) on a dry-weight basis. The physical properties and chemical analysis of the saline soil are detailed in Tables 1 and 2, respectively.

2.2. Soil Stabilizer. The saline soil has an extremely high content of soluble salt, especially chlorine and sulfate. According to the principles of hydration hardening of cement-based materials and the chemical excitation principles of binder materials, we designed a wide variety of proportions of curing agents by referencing previous studies and then tested their effectiveness in stabilizing the saline soil in Qinghai Province. After several optimizations and trials, we found that mixing ordinary Portland cement, fly ash, and ground granulated blast furnace slag in a certain proportion can provide the best curing effect. The soil stabilizer used in this study therefore consists of 20% Portland cement, 20% fly ash, and 60% ground granulated blast furnace slag by weight. The chemical compositions of these cementitious materials are given in Table 3.

2.3. Test Methods

2.3.1. Preparing, Curing, and Unconfined Compressive Strength (UCS) Testing of Specimens. The Sieved saline soil and the soil stabilizer were mechanically mixed. The mass of the soil stabilizer accounted for 10%, 15%, or 20% of the total weight of the dry sample, and then water was added. The mixing was continued until the fresh mixture became homogeneous. The water content was controlled to ensure that the sample reached the maximum dry density, that is, the optimum water content [32] The fresh mixture was then placed into a cylindrical mold with a 50 mm diameter and a 50 mm height and compacted to 100% of the maximum dry density. After being demolded, specimens were sealed in plastic bags and placed into a curing environment at a constant temperature of $20 \pm 2^{\circ}C$ and 100% relative humidity (standard curing conditions). The designed curing ages were 7 and 28 days. The specimens were taken out from the curing room 1 day before the designed age and saturated in water for 24 hours before UCS testing [33]. The level of water was about 2 cm higher than the top of the specimens. In the UCS testing, a constant loading rate was controlled at about 1 mm/min.

2.3.2. Test Methods for Freeze-Thaw Cycles of Stabilized Saline Soil. Since there is no standard method for evaluating the freeze-thaw resistance of stabilized soil in China at

Table 1: Physical properties of saline soil.

Plastic limit (%)	Liquid limit (%)	Plasticity index (%)	Optimum water content (%)	pH value of soil solution	Cl^- concentration of soil solution (mg/L)[b]	SO_4^{2-} concentration of soil solution (mg/L)[b]	Soluble salt content (%)
16.56	20.98	4.42	15.5	9.48	886.50	3326.20	4.0

[a]The solution was prepared at a mass rate of soil to deionized water ratio of 1 : 2.5. [b]The solution was prepared at a mass rate of soil to deionized water ratio of 1 : 10.

Table 2: Chemical composition of saline soil (% by weight).

Loss on ignition	SiO_2	Al_2O_3	CaO	Fe_2O_3	MgO	K_2O	Na_2O	SO_3	Cl^-	P_2O_5	Total
10.09	48.67	11.13	9.45	4.09	3.58	2.53	3.77	4.76	0.97	0.19	99.22

Table 3: Chemical analysis of Portland cement, slag, and fly ash (% by weight).

Materials	SiO_2	$A1_2O_3$	Fe_2O_3	CaO	MgO	Na_2O_{eq}	SO_3	Loss on ignition
Cement	22.80	4.55	2.82	65.34	2.74	0.55	2.92	3.90
Slag	34.63	13.92	0.29	38.28	10.52	—	0.25	0.25
Fly ash	57.60	21.90	7.70	3.87	1.68	0.41	4.05	0.43

present, and the testing methods of concrete are not suitable to adopt, this study modified and designed three test methods by referring to the ASTM D560-16 [34] freeze-thaw test method as follows.

Test I: Cyclic freeze-thaw test of all-round water supply to specimens without pressure. At the end of the curing period, the specimens, whose surfaces were wet, were placed into a moist room at a constant temperature of 20°C and relative humidity of 100%. After 24 hours, a water-saturated felt pad was placed between the specimens and the carriers, and the sample was placed in a freezing cabinet at a constant temperature of -25 ± 2°C for 12 hours. It was then moved to the moist room at a constant temperature of 20 ± 2°C and a RH >95% again to thaw for 11 hours. During the thawing period, all the side surfaces and upper top surface of the samples of saline soil were wetted by mist and then supplied with free water. In such a high relative humidity, we consider that the test samples were close to being soaked in water, so all the surfaces in contact with the mist had similar water supply conditions as the bottom surface of the specimen that was in contact with the felt pad. In every freezing and thawing step, it was necessary to keep the water-saturated felt pad in place, so sufficient potable water was available to permit the specimens to absorb water by capillary action.

To measure the mass loss of specimens after thawing, two firm strokes were given on all surfaces of each specimen with a wire scratch brush according to the method presented in ASTM D560-16. Before and after this step, the mass changes of specimens were recorded for calculating the percentage of cumulative mass loss (PCML). After brushing, the specimens were turned over endways before they were placed on the water-saturated pads.

The above procedures constitute one cycle (24 hours) of freezing and thawing. It should be noted that no extra pressure was applied in the process of supplying water to the specimens, which is different from the case when specimens are immersed into water where there is a pressure difference created by the water depth on the specimen surface.

Test II: Cyclic freeze-thaw test of unidirectional water supply to specimens without pressure. In this test, specimens from the curing storage were placed directly in sealed plastic bags, on the bottom of which one hole with a diameter of about 1 mm was created at the center of each specimen. In this test, a piece of water-saturated felt pad was always placed between the sealed bags holding the specimens and carriers, so that water could move to the bottom of each specimen through the holes.

The mass change of each specimen was measured every three cycles until thorough destruction took place. The water content of the specimens at a temperature of 105°C at the end of the curing period was recorded in order to obtain the critical value at the time when complete destruction occurred. If the mass increase is regarded as the increase of water content during freeze-thaw cycles, the critical water content can be calculated.

In Test II, the procedure continued as in Test I, but without giving two firm strokes on all areas of specimens and turning specimens over endways when they were placed on the water-saturated pad.

Test III: Cyclic freeze-thaw test without external water supply. In this test, specimens were placed in sealed plastic bags in order to separate them from moisture in the freezing and thawing steps. The remaining procedure continued in the same way as in Test II.

The water supply patterns in these three tests are sketched in Figure 1. In addition, other groups of specimens were cured under standard curing conditions with their strength determined simultaneously with the samples affected by the freeze-thaw cycles.

3. Results and Analysis

Experimental UCS data obtained from the three tests are given in Table 4.

3.1. Test I. Figure 2 shows the PCML of specimens in Test I. The changing patterns in UCS have a similar tendency to that in PCML. With increasing numbers of freezing-thawing

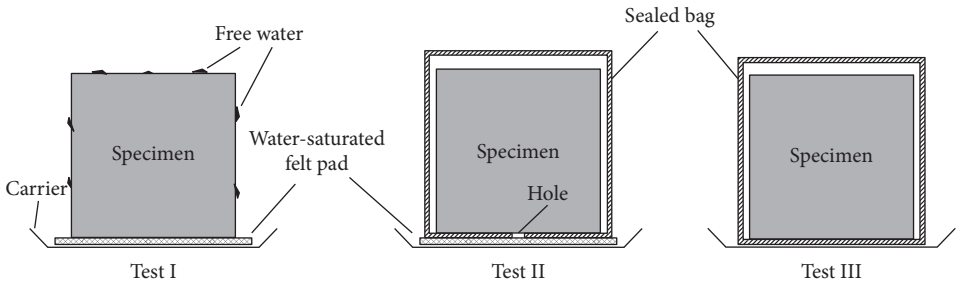

Figure 1: Sketch of the water supply conditions in the three tests.

Table 4: Changes in UCS of stabilized soil after freeze-thaw cycles in three tests.

Specimen group	Percent of stabilizer (%)	Age (days)	Initial strength[a] (MPa)	UCS after 12 cycles (MPa)				UCS after 24 cycles (MPa)				UCS after 60 cycles (MPa)			
				SS[b]	Test I	Test II	Test III	SS	Test I	Test II	Test III	SS	Test I	Test II	Test III
1	10	7	4.4	6.8	1.5	—[c]	4.4	9	—	—	2.1	9.5	—	—	1.2
2	15		5.4	8.3	2.6	3.9	5.9	9.9	—	—	3.6	11.2	—	—	2.9
3	20		7.1	9.8	3.9	4.9	6.9	11.1	—	—	5.4	13.5	—	—	5.0
4	10	28	7.1	9	3.6	5.1	7.1	9.5	2	2.6	5.6	9.8	—	1.0	4.0
5	15		10	9.9	5	5.8	10.0	11.7	2.8	6.2	7.3	12	—	5.1	7.4
6	20		10.7	11.4	5	6.3	10.3	13.1	4.8	6.9	8.9	14.4	3.5	6.5	7.6

[a]Initial strength means the value of the strength at the end of the curing period. [b]SS means the synchronous strength of the specimens cured under standard conditions. [c]— means the group of specimens were destroyed in or before this cycle.

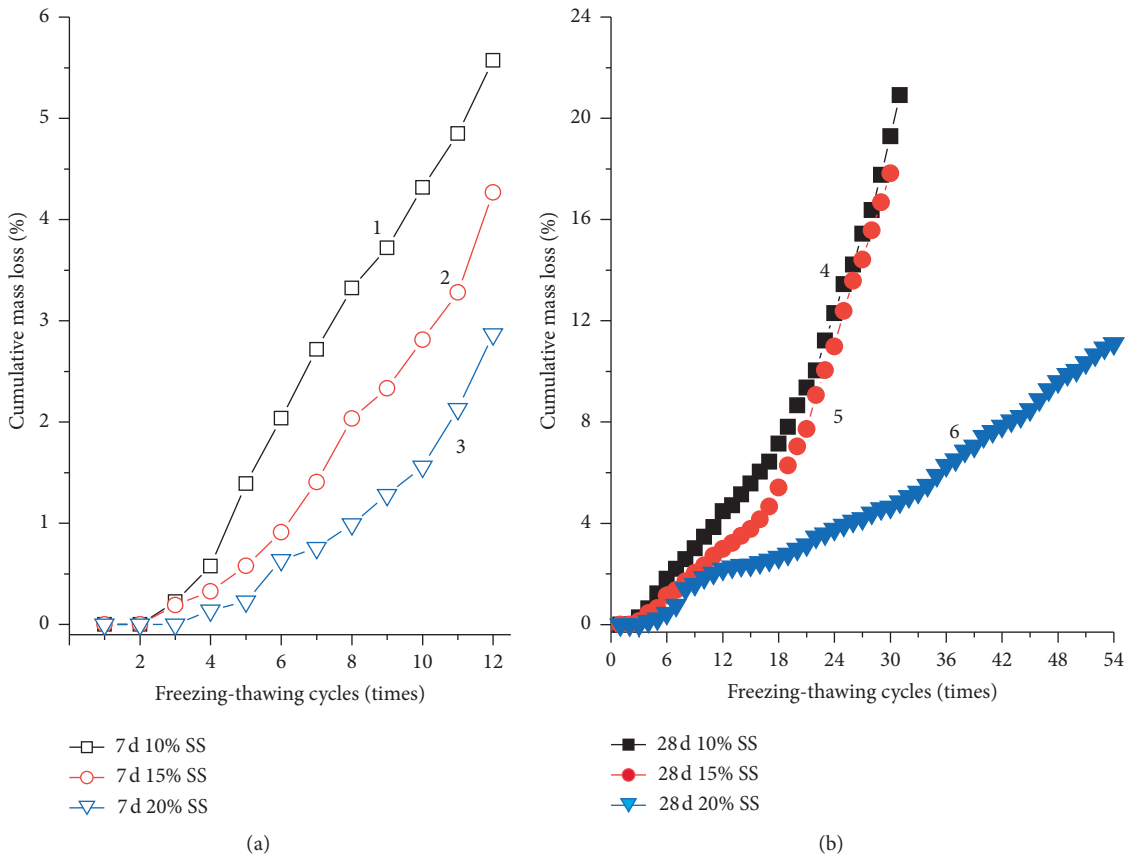

Figure 2: Cumulative mass loss of specimens with curing periods of 7 days (a) and 28 days (b) in Test I (SS means soil stabilizer).

cycles, the UCS decreases gradually until destruction occurs. The PCML of specimens with curing period of 7 days (specimen groups 1–3 in Table 4) begins to increase rapidly after five or six cycles. After eight or nine cycles, cracks appear one after another on these specimens. The failure patterns of these specimens are shown in Figure 3.

The UCS and PCML results reveal that the repeated freeze-thaw under the condition of all-round water supply to specimens has a strong destructive effect on the specimens with a short curing period. Furthermore, this destructive effect cannot be effectively reduced by increasing the content of the soil stabilizer. This is proved by the fact that the specimens stabilized by 20% stabilizer performed a little better than the ones with 10% stabilizer, yet they were destroyed completely after 12-18 cycles.

The PCML values of groups 4–6 with a curing period of 28 days were 5.5%, 3.8%, and 2.4%, respectively, at the end of the 15^{th} cycle and increased slowly. After 15 cycles, the PCML of group 6 specimens maintained a slow increase. However, for groups 4 and 5, the PCML of specimens started to rise steeply. Erosion in these specimens took place from the surface towards the core with water incursion, but visible cracks were hardly seen before 24 cycles. The PCML of specimens stabilized by 20% soil stabilizer did not exceed 5%, even after 30 cycles, and the UCS remained more than 3 MPa after 60 cycles. Therefore, a sufficiently long curing period is important to improve the freeze-thaw resistance of stabilized saline soil.

3.2. Test II. In this test, water migrated from the water-saturated felt pad to the center bottom of a specimen through a hole in an otherwise sealed bag. Similar to Test I, it is obvious that the freeze-thaw resistance of the specimens cured for short period is not as good as that for specimens cured for a longer period.

However, for the specimens with a curing term of 7 days, the failure pattern in Test II is distinctly different from that in Test I. In Test II, there was no obvious change in the mass and volume of specimens before six cycles. After six cycles, specimens of group 1 (10% stabilizer) began to rapidly expand in the upper part until the whole specimen fell apart to powder. The typical failure pattern of group 1 after night cycles is shown in Figure 4(a). The specimens of group 2 (15% stabilizer) and group 3 (20% stabilizer) still had 3-4 MPa UCS after 12 cycles but began to increase rapidly in mass and in volume after 12 cycles. The typical failure pattern of group 3 after 24 cycles is shown in Figure 4(b).

Conversely, the severe erosion phenomena did not show up in the specimens cured for 28 days. These specimens had no evident change in mass or appearance, even after 60 cycles. In Test II, the erosion extent of the specimens cured for 7 days exceeded that in Test I, while it was the opposite case for the specimens cured for 28 days. This conclusion can be deduced from the changes in UCS (Table 4).

3.3. Test III. In this test, specimens were separated from external moisture by sealed bags. The UCS data in Table 4 show that this had the least destructive effect on the stabilized soil specimens compared to the other two tests. However, the decreasing UCS data indicate that the destruction may be due to the salt in the soil.

4. Discussion

4.1. Failure Pattern of Specimens. As a result of rich sodium sulfate, large amounts of ettringite may form during hydration of the stabilizer-soil mixture (Figure 5; the rod-shaped phases are ettringites). However, in Test III, in addition to the negative influence of low temperature on potential activity of the soil stabilizer, crystallization of sulfate in the stabilized soil affected by repeated freeze-thaw is also a main cause of the reduction in the mechanical properties of specimens.

Despite many studies on the crystallization of sodium sulfate over the last 150 years, the reason why it generates damage remains controversial. Sodium sulfate has two stable phases at room temperature, thenardite (an anhydride) and mirabilite (a decahydrate), as well as a metastable phase [35–37]. At low temperature, the solubility of sodium sulfate largely decreases so that the pore liquid in the stabilized soil reaches supersaturation, which is a necessary condition for the occurrence of crystallization pressure [38, 39]. With decreasing temperature, both thenardite and mirabilite precipitate from a saturated sodium sulfate solution. Thenardite is the most abundant phase when precipitation occurs at low relative humidity in a porous material [40, 41]. As the temperature decreases and the amount of free water reduces, the salt concentration in the solution increases while the water activity decreases. A lower water activity is beneficial to the formation of thenardite. In micropores, precipitation of anhydrous sodium sulfate is promoted due to water activity reduction. Furthermore, crystallization of thenardite can generate tensile hoop stresses of the order of 10–20 MPa, which is higher than that caused by mirabilite at the same supersaturation ratios [42–44].

Figure 6 shows the changes in pore characteristics of specimens affected by freeze-thaw cycles in Test III. Curve 3 indicates that salt crystallization may be one of the factors that causes a higher porosity of specimens cured for short periods. Curve 2 appears close to Curve 1. This reveals that salt crystallization has little effect on specimens with a longer curing term after 12 cycles.

In Test III, the specimens are in a dry condition, which means only air is present in the macropores and mesopores, while any liquid tends to be in the micropores. Therefore, part of the sodium sulfate dissolves in the liquid in the micropores where the solution reaches a saturated state, and the rest of the sodium sulfate acts as part of the soil skeleton. The destructive effect is induced only from the sodium sulfate dissolved in the pore liquid, where crystallization of the sulfate and water can take place during the freeze-thaw cycles. The sulfate acting as the soil skeleton has little damage effect on the specimen given that there is no external moisture. In addition, the presence of a large volume of voids can relax the stress caused by crystallization of the salt and water. Arora et al. [45–47] pointed out that freeze-thaw cycles did not have any detrimental effect on cement-treated mixtures of

(a) (b)

Figure 3: Appearance of representative specimens of group 2 (a) and group 3 (b) after nine cycles in Test I.

(a) (b)

Figure 4: Appearance of representative samples of group 1 (a) after nine cycles and group 3 (b) after 24 cycles in Test II.

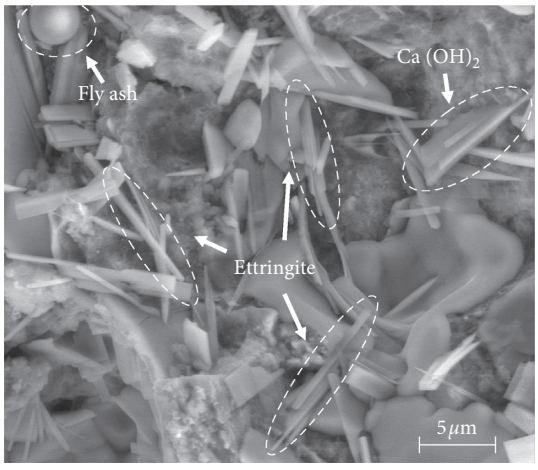

Figure 5: SEM image of saline soil stabilized by 15% stabilizer at an age of 7 days.

nonsaline sandy soil even though specimens were placed in a humidity chamber for thawing. Thus, the decrease in UCS shows the presence of the decay effect resulting from salt crystallization, but this effect is far slighter than those in Test I and Test II, where external water can invade specimens during the cyclic freeze-thaw process. Therefore, water content is a key factor in freeze-thaw damage of stabilized saline soil.

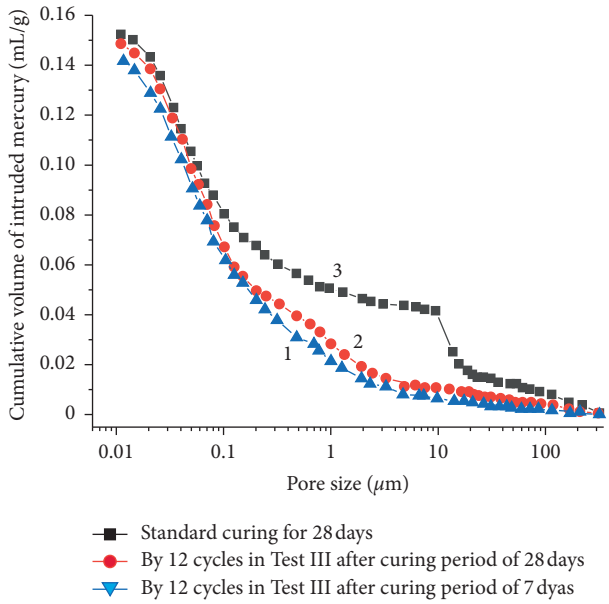

Figure 6: Pore size distribution of specimens stabilized by 10% stabilizer.

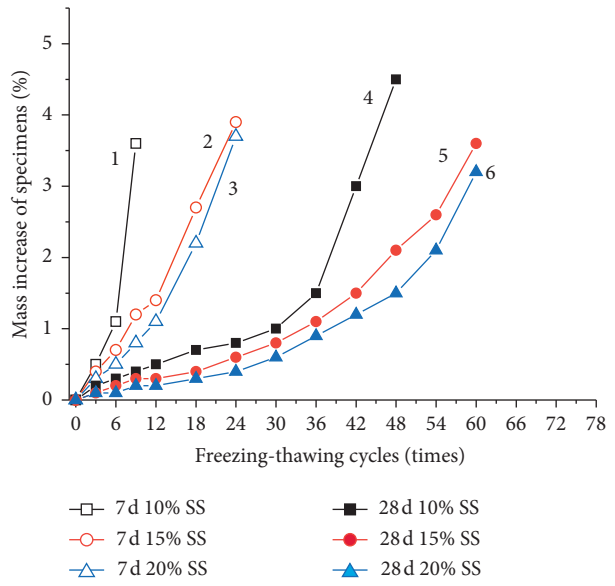

Figure 7: Percentage of mass increase of specimens in Test II (group 5 and 6 specimens were not destroyed completely after 60 cycles.).

In Test I and Test II, the freeze-thaw resistance of specimens cured for 28 days was much higher than that of specimens cured for 7 days. This is because the former specimens have a more compacted microstructure to prevent external water invasion. In addition, before repeated freezing and thawing, long-term curing is helpful for pozzolanic activity development of the soil stabilizer and for strength growth of specimens. Water intrusion damage is partly due to the expansion stress of ice. With increasing water content, more and more pores are filled with liquid, and thus the risk of frost damage grows. At the same time, more salt serving as part of the solid skeleton is dissolved into the pore liquid. This means that the salt solution in the specimen increases, and hence the zone influenced by the salt solution enlarges. When the temperature is lowered, crystallization of salts may cause serious damage to specimens. Moreover, the presence of moisture provides a necessary condition for growth of ettringite in the thawing steps. Expansion of ettringite can lead to serious damage in a hardened specimen.

When water content reaches a critical value, the specimen is rapidly destroyed in a freezing test. Figure 7 presents the percentage of mass increase of specimens in Test II. For the specimens cured for 7 days, when the percentage of mass increase reaches about 3.5%, corresponding with a water content of 18% (the water content of specimens is about 14.5% at the end of the curing period), complete destruction of the whole specimen occurs. For the specimens cured for 28 days, the critical value of percentage of mass increase is above 4.5%, corresponding with a water content of 20%. It should be noted that the time at which the water content of a specimen reaches a critical value is determined by its hydraulic conductivity. The longer the curing period, the lower the hydraulic conductivity that the specimen possesses.

As noted above, the specimens with short-term curing have two obviously different failure patterns under the conditions of all-round (Test I) and unidirectional (Test II) water supply to specimens. In Test I, erosion of specimens begins from the surface layers and goes on towards the core with water invading, until the whole specimen is separated into several blocks by the expanding crystal phases of water and salt (Figure 3). In Test II, expansion first takes place in the upper part of a specimen, followed by crushing of the whole specimen (Figure 4). The cause of the two failure patterns is related to the migration of external water into specimens and internal moisture within specimens during the freeze-thaw cycles.

4.2. Driving Force of Water Migration. In agrology, soil water potential is defined to characterize the total potential energy of water in soil. It can be defined as the Gibbs free energy in thermodynamics [48, 49]:

$$dG = V\,dP - S\,dT + \sum_{1}^{n} \frac{\partial G}{\partial ci} dci + \frac{\partial G}{\partial \theta}\theta + dw_g, \qquad (1)$$

where G is the Gibbs free energy, $V\,dP$ is the pressure potential caused by a change of pressure P, V is the volume, $-SdT$ is the temperature potential caused by a change of temperature T, and S is the entropy. The third term on the right-hand side of this equation is the solute potential caused by change in concentration c_i of the i^{th} kind of solute, the fourth term is the matric potential caused by change of water content θ, and dw_g is gravity potential. Potential gradient is the driving force of water migration. Soil water migrates along the normal direction of the equipotential plane from high potential to low potential.

When focusing on the problem of water migration in solidified soil, the gravity potential and solute potential in the

soil water potential can be ignored [21, 50]. As the influence created by temperature change on other aspects such as surface tension of water, matric potential, and pressure potential largely exceeds the change of temperature potential [51], especially for small-scale specimens in which the temperature gradient is small, the term -*SdT* can be ignored and other factors deserve more attention. Thus, (2) can be simplified as [52]

$$dG = VdP + \frac{\partial G}{\partial \theta} d\theta. \tag{2}$$

Matric potential is generated by the holding effect of the soil matric on moisture, which is dominated by either the adsorption effect at low water content or capillary attraction at high water content. Therefore, it is a function with respect to water content, θ. As the matric potential is a negative value, the term for soil water suction is defined as its opposite number. Soil water suction, F_{su}, can be expressed as

$$F_{su} = -\frac{\partial G}{\partial \theta} d\theta = a\left(\frac{\theta}{\theta s}\right)^{b}, \tag{3}$$

where θs is the saturation water content, and a and b are empirical constants. Equation (3) indicates that soil water suction has a decreasing power relation with water content before the saturated water content is reached. In [53], it was found experimentally that soil water potential in frozen soil increases at a power rate with decreasing temperature. According to (3), it can be explained by equivalently decreasing the water content when the liquid water in pores turns gradually into ice at low temperatures. Furthermore, soil water suction is also elevated due to increasing surface tension with decreasing temperature.

Before freezing, external water tends to be sucked into the specimen by a matric potential gradient between the surface and the core of the specimen when the specimen is in contact with water. When freezing, external water first ices. Due to the surface energy effect of soil particles on water and the salt dissolving in the water, the freezing point of water in the specimen decreases, so the external water source supply is shut off. Consequently, not much water enters the specimen during the freezing step. When thawing, the thawing front progresses from the outside towards the core of the specimen. The outer side of this thawing front maintains a relatively low water content and thereby a higher soil water suction compared with the inner side, where thawed liquid is sucked towards the outer side of the thawing front. Thus, water suction occurs with a progressing thawing front mainly during the thawing step.

4.3. Patterns of Water Migration. The similarity between Tests I and II is the pressure-free water supply; i.e., no extra water pressure or air pressure is applied throughout the testing process. Besides, the difference between these two tests is that Test I adopts the all-round method of water supply to ensure there is sufficient free water on the surface of the specimens, whereas Test II supplies limited water in one direction from the bottom of samples, and the other surfaces of samples are always in a dry state.

In Test I, no extra pressure is exerted on specimens except for atmospheric pressure when water is supplied from all directions. Therefore, air in the pores of the core of the specimen is sealed by water on the surface and cannot escape. Figure 8(a) sketches external water migration in connected pores from the surface towards the core under the conditions of Test I. Before freezing, external water is sucked from the surface of the specimen through capillaries. By assuming that the solidified soil is an isotropic material, considering only the connected pores from the surface to the inside, and assuming cylindrical capillaries, a model of external water invading the specimen is as given in Figure 8(b), where water in the specimen is neglected due to the low water content, resulting in the macropores and mesopores being in an almost dry state.

If gravity action is not considered, soil water potential consists of matric potential and pressure potential. The intruding water compresses the air, so the inner pressure increases. When the pressure difference between the inner and outer parts equals the additional pressure created by the concave meniscus in the capillary, the external water stops intruding. The pressure difference can be expressed by the Young-Laplace equation:

$$\Delta P = P - P_0 = \gamma\left(\frac{1}{R_1} + \frac{1}{R_2}\right), \tag{4}$$

where P is the inner air pressure, P_0 is the external atmospheric pressure, γ is the surface tension of water, and R_1 and R_2 are two radii of the meniscus curvature. The inner air pressure can be estimated by the ideal gas law equation:

$$PV = nRT, \tag{5}$$

where n is the number of moles of air and R is the ideal gas constant. Before the beginning of the freezing step, the inner air may be regarded as being under isothermal compression. Therefore, the change of air volume can be obtained from

$$\Delta V = \frac{V_0(P_0 - P)}{P} = -\frac{\Delta P V_0}{(P_0 + \Delta P)}, \tag{6}$$

where V_0 is the original volume of the inner air, corresponding with pressure P_0. The absolute value of ΔV is the volume of intruded water, ΔV_w:

$$\Delta V_w = \frac{V_0}{\left(1 + P_0/\left(\gamma\left(1/R_1 + 1/R_2\right)\right)\right)}. \tag{7}$$

When the temperature is lowered to T_2, which is above the freezing point of the external water, the inner air shrinks until the pressure difference can balance the additional pressure from the concave meniscus. The volume of intruded water can be calculated according to

$$\Delta V_w = V_0\left(1 - \frac{P_0 T_2}{T_0\left(P_0 + \gamma\left(1/R_1 + 1/R_2\right)\right)}\right). \tag{8}$$

Furthermore, γ increases with decreasing temperature, which promotes water intrusion. V_0 can be estimated according to

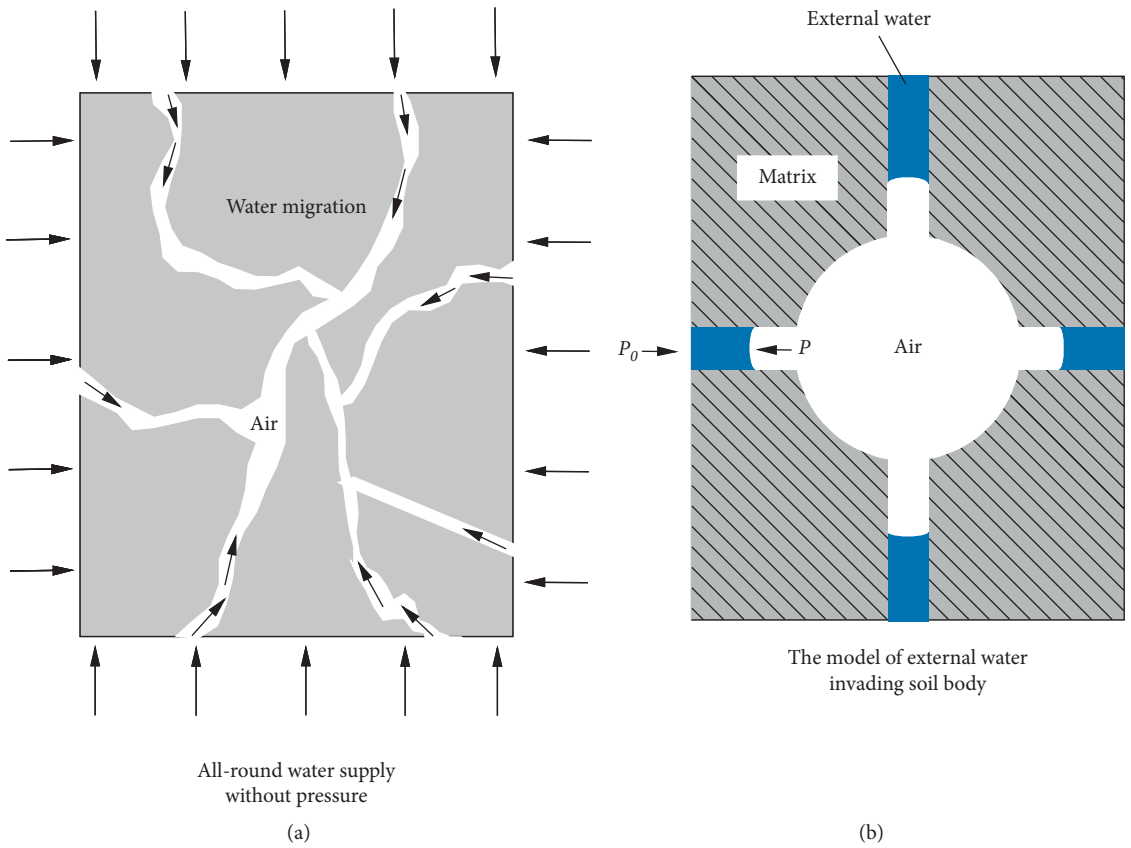

Figure 8: Sketch of water migration and the simplified model of Test I.

$$V_0 = V_{sp} - \frac{m_s}{\rho_s} - \frac{m_l}{\rho_l}, \tag{9}$$

where V_{sp} is the volume of the specimen, m_s and m_l are the dry mass and moist mass, respectively, of the specimen at the end of curing, and ρ_s and ρ_l are the density of soil particles and the density of water, respectively.

Once freezing occurs, external water cannot intrude any more, even though the inner air pressure continues to decrease and soil water suction increases. However, the negative/suction pressure generated is the driving force that sucks free water from the thawing front in the thawing step.

In Test I, due to the presence of this air pressure potential, external water is kept out of the specimen core and accumulates only in the outer part, where the microstructure of the specimen is firstly eroded. This is why erosion takes place from the surface towards the core in Test I. With a short curing period, the pozzolanic reactivity of the soil stabilizer cannot fully develop. Therefore, the specimen is not compact enough, and there are some big flaws in the microstructure, through which external water can intrude the core of the specimen. An uncompacted microstructure leads to high hydraulic conductivity. Accordingly, these specimens fail early. This is why the specimens cured for a short period are destroyed as in Figure 3.

Unlike Test I, no pressure potential appears under the experimental condition of unidirectional water supply to specimens because the pressure in pores connected with air always equals atmospheric pressure. Thus (2) can be further simplified to

$$dG = \frac{\partial G}{\partial \theta} d\theta + dw_g. \tag{10}$$

Equation (10) reveals that the water migration depends on the gradient of the matric potential and the gravity potential. In Test II, water migrates from the bottom of the specimen upwards. Figure 9 sketches the water migration and water content distribution in the specimen under this condition. Since water content in the top part is always lower than that in the bottom part before the whole specimen reaches saturation, the gradient of matric potential always drives water upwards.

Since external water is obtained only through the hole from the water-saturated felt pad, it is not sufficient, and the intruded water is fully dispersed in the specimen due to the action of soil water suction. Therefore, the water content even in the bottom part cannot reach the critical value at which the specimen is completely destroyed, and the bottom can keep sucking water from the environment.

Thus, each part of the specimen strives to acquire water to reach the balance of the soil water potential, leading to full dispersion of water in the whole specimen. Therefore, it is difficult to accumulate water in some parts, for example, the bottom. This is why the destructive phenomenon of specimens under this condition occurs later than that under the conditions of all-round water supply to specimens. Only when the

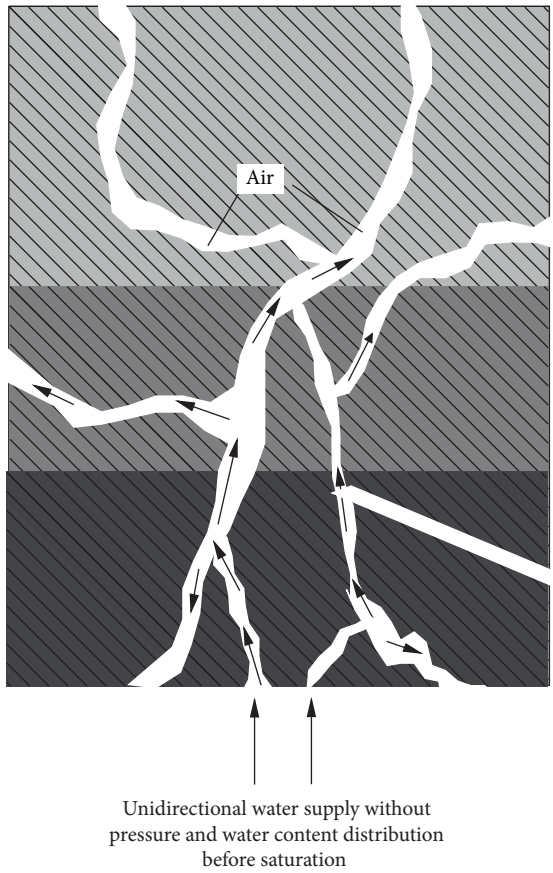

Figure 9: Sketch of water migration and water content distribution before saturation in Test II.

water content in the whole specimen synchronously reaches the critical value, will frost damage suddenly occur.

When water content in the matric is low, the holding effect on water mainly depends on adsorption. Therefore, the method of capillary rise is not suitable for estimation of intruded water. With increasing water content, more sodium sulfate dissolves into the pore liquid and then rises to the upper part, together with migrating moisture. Expansion and destruction of specimens occur firstly in the upper part, which proves that cumulative salt in the pore liquid is the most significant cause leading to specimen failure in Test II. After 12 cycles, the content of the dissoluble salt in the upper and lower halves of specimens belonging to group 2 was measured. The results revealed that the salt content in the lower half was only 81% of that in the upper half, which confirms that the salt moved from the lower part and accumulated in the upper part during the cyclic freeze-thaw processes. Moreover, the uneven distribution of salt may produce osmotic potential and then further affect the migration of water.

5. Conclusion

By designing three test methods for freeze-thaw cycles of stabilized saline soil, this study has investigated the freeze-thaw resistance of saline soil stabilized by cement-based material under different types of water supply. It has also analyzed the failure modes of the specimens and the role of salt and water in the freezing and thawing process. The concept of soil water potential has been introduced, and the dynamic mechanism and migration of water and salt have been described through theoretical models. The effect of water content on the freeze-thaw resistance of stabilized saline soil has also been discussed. The main conclusions of this study are as follows.

In cyclic freeze-thaw tests, external water is one of the most important factors in the destruction of stabilized saline soil. Different failure patterns are caused by different water supply patterns in freeze-thaw tests. If no external water is supplied, specimens have no obvious appearance of erosion, even though the UCS gradually decreases with increasing number of freeze-thaw cycles.

Under the condition of all-round water supply to specimens, the pressure potential caused by the inner air leads to water accumulating first in the outer part of the specimen. For specimens with a long-term curing period, erosion from the surface towards the core is a distinct characteristic of the failure pattern.

Under the condition of unidirectional water supply to specimens, air pressure potential is eliminated and

matric potential drives moisture to migrate from the bottom upwards, finally dispersing all over the specimen. The sulfate in the lower part of the specimen is dissolved and then carried to the upper part. Gradual accumulation of salt causes the specimen to turn into powder when a certain water content is reached.

The water content is an important factor for appearance of macroscopical frost damage. In this study, the estimated critical value of water content was about 18%–20%.

The pozzolanic reactivity of soil stabilizer is reduced by low temperature. A high percentage of soil stabilizer can improve the freeze-thaw resistance of stabilized soil, but a sufficiently long curing period plays a more important role.

Abbreviations

a and b: Empirical constants
c_i : Concentration of the i^{th} kind of solute
F_{su}: Soil water suction
G: Gibbs free energy, J
m_s and m_l: Specimen dry mass and moist mass at end of curing, kg
n: Number of moles of air
P: Air pressure, Pa
P_0: External atmospheric pressure, Pa
R: Ideal gas constant
R_1 and R_2: Radii of meniscus curvature, m
r: Pore radius, m
S: Entropy
T: Temperature, K
T_2: Final temperature, K
V: Air volume, m^3
V_{sp}: Volume of specimen, m^3
V_0: Original volume of inner air, m^3
w_g: Work done by gravity on water, J
α_{H2O}: Water activity
γ: Surface tension of water, mN/m
ΔV: Volume difference of air of intruded water, m^3
ΔV_w: Volume of intruded water, m^3
θ: Water content of soil body
θ_s: Saturation water content
ρ_s and ρ_l: Density of soil particles and density of water, kg/m^3.

Data Availability

All the data included in this study are available upon request by contacting the corresponding author.

Conflicts of Interest

The authors declare that there are no conflicts of interest regarding the publication of this paper.

Acknowledgments

This work was supported by a grant from National Key R&D Program of China 2018YFD1101002.

References

[1] S. Zhang, J. Zhang, Y. Gui, W. Chen, and Z. Dai, "Deformation properties of coarse-grained sulfate saline soil under the freeze-thaw-precipitation cycle," *Cold Regions Science and Technology*, vol. 177, Article ID 103121, 2020.

[2] B. Yang, Z. Qin, Q. Zhou, H. Li, L. Li, and X. Yang, "Pavement damage behaviour of urban roads in seasonally frozen saline ground regions," *Cold Regions Science and Technology*, vol. 174, Article ID 103035, 2020.

[3] H. Li, Y. Lai, L. Wang et al., "Review of the state of the art: interactions between a buried pipeline and frozen soil," *Cold Regions Science and Technology*, vol. 157, pp. 171–186, 2019.

[4] H. Li, Y. Lai, and L. Li, "Impact of hydro-thermal behaviour around a buried pipeline in cold regions," *Cold Regions Science and Technology*, vol. 171, Article ID 102961, 2020.

[5] H. Zhang, X. Yuan, Y. Liu, J. Wu, X. Song, and F. He, "Experimental study on the pullout behavior of scrap tire strips and their application as soil reinforcement," *Construction and Building Materials*, vol. 254, Article ID 119288, 2020.

[6] S. M. Hejazi, M. Sheikhzadeh, S. M. Abtahi, and A. Zadhoush, "A simple review of soil reinforcement by using natural and synthetic fibers," *Construction and Building Materials*, vol. 30, pp. 100–116, 2012.

[7] S. Zhang, X. Yang, S. Xie, and P. Yin, "Experimental study on improving the engineering properties of coarse grain sulphate saline soils with inorganic materials," *Cold Regions Science and Technology*, vol. 170, Article ID 102909, 2020.

[8] Y. Liu, Q. Wang, S. Liu et al., "Experimental investigation of the geotechnical properties and microstructure of lime-stabilized saline soils under freeze-thaw cycling," *Cold Regions Science and Technology*, vol. 161, pp. 32–42, 2019.

[9] Q. Lv, L. Jiang, B. Ma, B. Zhao, and Z. Huo, "A study on the effect of the salt content on the solidification of sulfate saline soil solidified with an alkali-activated geopolymer," *Construction and Building Materials*, vol. 176, pp. 68–74, 2018.

[10] P. Sargent, *The Development of Alkali-Activated Mixtures for Soil Stabilisation*, Woodhead Publishing Limited, Sawston, UK, Cambridge, 2015.

[11] M. Naveed, J. Duan, S. Uddin, M. Suleman, Y. Hui, and H. Li, "Application of microbially induced calcium carbonate precipitation with urea hydrolysis to improve the mechanical properties of soil," *Ecological Engineering*, vol. 153, Article ID 105885, 2020.

[12] T. Zhang, Y.-L. Yang, and S.-Y. Liu, "Application of biomass by-product lignin stabilized soils as sustainable Geomaterials: a review," *Science of the Total Environment*, vol. 728, Article ID 138830, 2020.

[13] C. Zhang, D. Li, J. Jiang et al., "Evaluating the potential slope plants using new method for soil reinforcement program," *Catena*, vol. 180, pp. 346–354, 2019.

[14] F. Kalantary and M. Kahani, "Evaluation of the ability to control biological precipitation to improve sandy soils," *Procedia Earth and Planetary Science*, vol. 15, no. 21, pp. 278–284, 2015.

[15] L. A. van Paassen, C. M. Daza, M. Staal, D. Y. Sorokin, W. van der Zon, and M. C. M. Van Loosdrecht, "Potential soil reinforcement by biological denitrification," *Ecological Engineering*, vol. 36, no. 2, pp. 168–175, 2010.

[16] W. Zhang, J. Ma, and L. Tang, "Experimental study on shear strength characteristics of sulfate saline soil in Ningxia region under long-term freeze-thaw cycles," *Cold Regions Science and Technology*, vol. 160, pp. 48–57, 2019.

[17] C. C. Ikeagwuani and D. C. Nwonu, "Emerging trends in expansive soil stabilisation: a review," *Journal of Rock Mechanics and Geotechnical Engineering*, vol. 11, no. 2, pp. 423–440, 2019.

[18] F. Wang, X. Qin, and R. Sun, "The investigation of concrete durability under natural condition of Caerhan Salt Lake," *Bulletin of the Chinese Ceramic Society*, vol. 4, no. 21, pp. 16–22, 2002.

[19] A. Mardani-Aghabaglou, İ. Kalıpcılar, G. İnan Sezer, A. Sezer, and S. Altun, "Freeze-thaw resistance and chloride-ion penetration of cement-stabilized clay exposed to sulfate attack," *Applied Clay Science*, vol. 115, pp. 179–188, 2015.

[20] X. Long, G. Cen, L. Cai, and Y. Chen, "Model experiment of uneven frost heave of airport pavement structure on coarse-grained soils foundation," *Construction and Building Materials*, vol. 188, pp. 372–380, 2018.

[21] J. Zhang, Y. Lai, J. Li, and Y. Zhao, "Study on the influence of hydro-thermal-salt-mechanical interaction in saturated frozen sulfate saline soil based on crystallization kinetics," *International Journal of Heat and Mass Transfer*, vol. 146, Article ID 118868, 2020.

[22] X. Wan, Q. Hu, and M. Liao, "Salt crystallization in cold sulfate saline soil," *Cold Regions Science and Technology*, vol. 137, pp. 36–47, 2017.

[23] X. Zhao, A. Shen, Y. Guo, P. Li, and Z. Lv, "Pavement mechanic response of sulfate saline soil subgrade section based on fluid-structure interaction model," *International Journal of Pavement Research and Technology*, vol. 10, no. 6, pp. 497–506, 2017.

[24] D. Wu, Y. Lai, and M. Zhang, "Thermo-hydro-salt-mechanical coupled model for saturated porous media based on crystallization kinetics," *Cold Regions Science and Technology*, vol. 133, pp. 94–107, 2017.

[25] R. Bai, Y. Lai, M. Zhang, and J. Ren, "Study on the coupled heat-water-vapor-mechanics process of unsaturated soils," *Journal of Hydrology*, vol. 585, Article ID 124784, 2020.

[26] D. Wang, Q. Wang, and Z. Huang, "New insights into the early reaction of NaOH-activated slag in the presence of CaSO4," *Composites Part B: Engineering*, vol. 198, Article ID 108207, 2020.

[27] S. Zhuang and Q. Wang, "Inhibition mechanisms of steel slag on the early-age hydration of cement," *Cement and Concrete Research*, vol. 140, Article ID 106283, 2021.

[28] J. Liu, P. Yang, and Z. Yang, "Electrical properties of frozen saline clay and their relationship with unfrozen water content," *Cold Regions Science and Technology*, vol. 178, no. 159, Article ID 103127, 2020.

[29] Q. Wang, J. Qi, S. Wang, J. Xu, and Y. Yang, "Effect of freeze-thaw on freezing point of a saline loess," *Cold Regions Science and Technology*, vol. 170, Article ID 102922, 2020.

[30] J. Xu, Y. Li, W. Lan, and S. Wang, "Shear strength and damage mechanism of saline intact loess after freeze-thaw cycling," *Cold Regions Science and Technology*, vol. 164, Article ID 102779, 2019.

[31] R. Tang, G. Zhou, J. Wang, G. Zhao, Z. Lai, and F. Jiu, "A new method for estimating salt expansion in saturated saline soils during cooling based on electrical conductivity," *Cold Regions Science and Technology*, vol. 170, Article ID 102943, 2020.

[32] J. Ren, "The damage mechanism and failure prediction of concrete under wetting-drying cycles with sodium sulfate solution," *Construction and Building Materials*, vol. 264, Article ID 120525, 2020.

[33] RIOH, Test Methods of Materials Stabilized with Inorganic Binders for Highway Engineering (JTG E51–2009), 2009.

[34] ASTM International, Methods for Freezing and Thawing Compacted Soil-Cement Mixtures, 2016.

[35] J. Ren, Y. Lai, R. Bai, and Y. Qin, "The damage mechanism and failure prediction of concrete under wetting-drying cycles with sodium sulfate solution," *Construction and Building Materials*, vol. 264, Article ID 120525, 2021.

[36] Y. Wang, I.-M. Chou, M. Zheng, and X. Hou, "Acquisition and evaluation of thermodynamic data for mirabilite-thenardite equilibria at 0.1 MPa," *The Journal of Chemical Thermodynamics*, vol. 111, pp. 221–227, 2017.

[37] A. I. Vavouraki and P. G. Koutsoukos, "Kinetics of crystal growth of mirabilite in aqueous supersaturated solutions," *Journal of Crystal Growth*, vol. 338, no. 1, pp. 189–194, 2012.

[38] P. Vazquez, C. Thomachot-Schneider, K. Mouhoubi et al., "Sodium sulfate crystallisation monitoring using IR thermography," *Infrared Physics & Technology*, vol. 89, pp. 231–241, 2018.

[39] T. A. Saidov, L. Pel, and G. H. A. Van Der Heijden, "Crystallization of sodium sulfate in porous media by drying at a constant temperature," *International Journal of Heat and Mass Transfer*, vol. 83, pp. 621–628, 2015.

[40] P. A. J. Donkers, K. Linnow, L. Pel, M. Steiger, and O. C. G. Adan, "Na2SO4·10H2O dehydration in view of thermal storage," *Chemical Engineering Science*, vol. 134, pp. 360–366, 2015.

[41] C. Rodriguez-Navarro, E. Doehne, and E. Sebastian, "How does sodium sulfate crystallize? Implications for the decay and testing of building materials," *Cement and Concrete Research*, vol. 30, no. 10, pp. 1527–1534, 2000.

[42] R. J. Flatt, "Salt damage in porous materials: how high supersaturations are generated," *Journal of Crystal Growth*, vol. 242, no. 3-4, pp. 435–454, 2002.

[43] E. M. Winkler and P. C. Singer, "Crystallization pressure of salts in stone and concrete," *Geological Society of America Bulletin*, vol. 83, no. 11, pp. 3509–3514, 1972.

[44] G. W. Scherer, "Stress from crystallization of salt," *Cement and Concrete Research*, vol. 34, no. 9, pp. 1613–1624, 2004.

[45] S. Arora and A. H. Aydilek, "Class F fly-ash-amended soils as highway base materials," *Journal of Materials in Civil Engineering*, vol. 17, no. 6, pp. 640–649, 2005.

[46] M. H. Gorakhki and C. A. Bareither, "Unconfined compressive strength of synthetic and natural mine tailings amended with fly ash and cement," *Journal of Geotechnical and Geoenvironmental Engineering*, vol. 143, no. 7, 2017.

[47] I. Bozbey, M. K. Kelesoglu, B. Demir et al., "Effects of soil pulverization level on resilient modulus and freeze and thaw resistance of a lime stabilized clay," *Cold Regions Science and Technology*, vol. 151, pp. 323–334, 2018.

[48] J. W.. Gibbs, "A method of geometrical representation of the thermodynamic properties of substances by means of surfaces," *Transactions of Connecticut Academy of Arts and Sciences*, vol. 8, pp. 382–404, 1873.

[49] X. Zhao, Study on Water-Salt Transport and HTSPE Coupled Model of the Saline Soil in Western Jilin, 2018.

[50] Z. Li, Q. Xue, T. Katsumi, and T. Inui, "Electric-hydraulic-chemical coupled modeling of solute transport through

landfill clay liners," *Applied Clay Science*, vol. 101, pp. 541–552, 2014.
[51] Z. D. Lei, S. X. Yang, and S. C. Xie, Kinetic of Soil Wate, 1988.
[52] Y. D. Qin, Soil physics Encyclopedia of Earth Sciences Series, pp. 686–693, 2003.
[53] Y. Ji, G. Zhou, X. Zhao et al., "On the frost heaving-induced pressure response and its dropping power-law behaviors of freezing soils under various restraints," *Cold Regions Science and Technology*, vol. 142, pp. 25–33, 2017.